ROYAL SOCIETY
OF CHEMISTRY

PAPER

Check for updates

High response photochromic films based on D–A diarylethenes and their application in holography†

Maria Chiara Mantero,[a] Luca Oggioni,[a] Giorgio Pariani,[a] Fausto Ortica, [bc]
Silvano Tosi,[de] Maurizio Canepa,[f] Chiara Bertarelli, [gh] Matteo Tommasini [g]
and Andrea Bianco [*a]

A set of photochromic dithienylethenes bearing amino and nitro groups are synthesised and embedded at high concentrations in a polymer matrix (Cellulose Acetate Butyrate, CAB) to produce films showing a large reversible modulation of the complex refractive index in the Vis–NIR spectral range, thanks to an interesting combination of remarkable response at the molecular level and very high load capability in the chosen matrix. The photochromic derivatives are characterized in solution and in CAB films by means of electronic and vibrational spectroscopy, complemented by DFT calculations. Both the real and imaginary part of the refractive index are determined by spectroscopic ellipsometry. The modulation of the refractive index in the near infrared is in the range 0.02–0.04. These are very large values for such kinds of systems and they are due to a favourable combination of very large solubility of the derivatives in CAB and a high polarisability change. As for the change in transparency in the visible, contrast values larger than 10^3 are easily achieved. Based on such films, holograms are written and reconstructed with a very high fidelity and efficiency.

Introduction

Nowadays, photochromic materials are considered in a broad perspective as light switches of microscopic and macroscopic properties. The modulation and control of fluorescence are widely studied[1–4] for their potential use in high-resolution microscopy;[5,6] the mechanical effect has also been highlighted[7–9] and other examples include the use of photochromic molecules in photopharmacology and to trigger specific functions in biological systems.[10,11]

[a]INAF – Osservatorio Astronomico di Brera, Via Bianchi 46, 23807, Merate, Italy. E-mail: andrea.bianco@inaf.it

[b]Dipartimento di Chimica, Biologia e Biotecnologie, Università Degli Studi di Perugia, Via Elce di Sotto 8, Perugia, 06123, Italy

[c]Istituto Nazionale di Fisica Nucleare (INFN), Sezione di Perugia, Via Pascoli, Perugia, 06123, Italy

[d]Dipartimento di Fisica, Università di Genova, Via Dodecaneso 33, Genova, 16146, Italy

[e]INFN, Sezione di Genova, Via Dodecaneso 33, Genova, 16146, Italy

[f]OPTMATLAB, Dipartimento di Fisica, Università di Genova, Via Dodecaneso 33, Genova, 16146, Italy

[g]Dipartimento di Chimica, Materiali e Ingegneria Chimica, Politecnico di Milano, Piazza Leonardo da Vinci 32, 20133, Milano, Italy

[h]Center for Nano Science and Technology, Istituto Italiano di Tecnologia, Via Pascoli 10, 20133, Milano, Italy

† Electronic supplementary information (ESI) available: IR spectra of two derivatives, trend of complex refractive index of two derivatives. See DOI: 10.1039/d0ra05535b

In spite of such broader application spectrum, the optical field remains a key one where photochromic systems are valuable. In particular, this is the case of holography and holographic optical elements (HOEs).[12–14]

An HOE is a diffractive element that is produced by means of holography[15] and that allows the production of very different optical functions, such as light focusing, light diffusing and 3D imaging, paving the way to new conceptual optical designs that are thin, light and efficient. Their principle of work is the diffraction by a periodic modulation of transparency and/or the refractive index impressed in the photosensitive material. Moreover, their diffraction efficiency is directly related to the modulation of transparency and refractive index.[16,17]

It is apparent how photochromic materials are good candidates for such application thanks to their reversible modulation of both transparency and refractive index.[18] In particular, diarylethenes have a prominent role. Since the discovery of their photochromic properties by Irie,[19,20] they have become the reference P-type photochromic materials with high fatigue resistance, high quantum yields and remarkable photochromic properties in solid phase (crystal and amorphous).[21] Indeed, diarylethenes have been used in high response polymeric films.[22–25] In these systems, it was demonstrated that changes in transparency and refractive index were remarkable[18] if backbone photochromic polymers were used.[26] Thanks to that, diarylethene-based HOEs have already been reported in the literature.[27,28]

To foster the application of photochromic molecules in holography, it would be highly desirable to find a good combination of diarylethene derivatives with peculiar structure and polymer matrix showing a very large solubility and modulation of optical properties.

Here we report about three dithienylethene derivatives that are very soluble in the CAB matrix and that are functionalised with donor and/or acceptor functional groups. Such molecules are designed to enhance the absorption properties and the refractive index modulation, thus improving the performance of the holograms. The study of the photochromic and spectroscopic performances is carried out in solution and then in the CAB matrix. We show the potential application of such systems in real devices by producing reliable phase and amplitude computer-generated holograms with performance comparable or better than that of backbone photochromic polymers.

Materials and methods

The three molecules considered feature the same basic structure, namely the 1,2 dithienylperfluorocyclopentene, functionalized with different side groups (R₁ and R₂) in the *para* position of the phenyl ring: two electron donor groups (dimethylaniline, diphenylaniline) and one electron acceptor group (nitrophenyl). Fig. 1 reports the chemical structure of the three derivatives in their open form, which is uncoloured, and the corresponding names used throughout the paper.

Notably, the two symmetric molecules, have been already reported in the literature for improving the cycloreversion by means of a complexation (**AmAm**)[29] and for the development of anti-counterfeiting inks (**TrfAm**),[30] showing the effect on the switching properties. The asymmetric derivative (**NtAm**) was study from a theoretical point of view to evaluate the nonlinear optical properties.[31]

Chemical synthesis and film preparation

The synthesis of the molecules followed a Suzuki cross-coupling between 1,2-bis-(5-chloro-2-methyl-3-thienyl)hexafluorocyclo-pentene and commercial available boronic acids or pinacol esters,[32] by catalysis with Pd(PPh₃)₄ or X-Phos and Pd(OAc)₂.[33]

Unless otherwise specified, all reagents, catalysts, solvents were commercial (Sigma-Aldrich, Alfa Aesar, Frontier Scientific). All reactions of air–water-sensitive reagents and intermediates were carried out in dried glassware and argon atmosphere. Solvents were previously dried by means of conventional methods and stored under argon. NMR spectra were recorded on a Bruker AXR 400 spectrometer at 400 MHz. Mass spectra were recorded on a Bruker Esquire 3000 plus.

AmAm. 1,2-Bis-(5-chloro-2-methyl-3-thienyl)hexafluorocyclopentene (0.250 g, 0.57 mmol), 4-(N,N-dimethylamino)phenyl-boronic acid (0.226 g, 1.37 mmol), Pd(OAc)₂ (0.005 g, 0.022 mmol), X-Phos (0.013 mg, 0.027 mmol), nBuOH (3 mL, degassed), and a solution of NaOH (0.075 mg, 1.86 mmol) in water (0.8 mL, degassed) were subsequently added to a reaction flask under inert atmosphere. The reaction was stirred for 1 hour at ambient temperature, and for a further hour at 40 °C to favour the dissolution of 1,2-bis-(5-chloro-2-methyl-3-thienyl) hexafluorocyclopentene. The mixture was poured into water, and extracted with ethyl acetate. The combined organic layers were dried over Na₂SO₄, and, after solvent removal, the raw product was purified by flash chromatography on alumina (petroleum ether : ethyl acetate, 1 : 0 to 19 : 1 v/v). Powder of the desired compound (0.125 g, 0.21 mmol) was obtained in 36% yield.

^{1}H-NMR (CDCl₃) δ ppm: 7.43 (4H, Ph-H, d, $J = 8.8$ Hz), 7.12 (2H, Th-H, s), 6.74 (4H, Ph-H, br d, $J = 7.8$ Hz), 3.00 (6H, –N(CH₃)₂, s), 1.94 (6H, –CH₃, s).

^{13}C-NMR (101 MHz, CDCl₃) δ ppm: 150.19, 142.88, 139.22, 126.58, 125.73, 121.89, 120.05, 112.55, 40.46, 14.44.

ESI-MS: m/z 607.2 [M + H⁺].

NtAm. 1,2-Bis-(5-chloro-2-methyl-3-thienyl)hexafluorocyclopentene (0.500 g, 1.14 mmol), 4-(N,N-dimethylamino)phenyl-boronic acid (0.265 g, 1.60 mmol), 4-nitrophenylboronic acid pinacol ester (0.455 g, 1.83 mmol), Na₂CO₃·10H₂O (0.725 g, 6.84 mmol), Pd(PPh₃)₄ (0.139 g, 0.12 mmol), dimethoxyethane (DME, 16 mL, degassed), and water (8 mL, degassed) were subsequently added to a reaction flask, and processed by microwave at 140 °C for 1 hour. After cooling to room temperature, the mixture was poured into water, and extracted with diethyl ether. The combined organic layers were dried over Na₂SO₄, and, after solvent removal, the raw product was purified by flash chromatography on alumina (petroleum ether : dicloro methane, 1 : 0 to 1 : 2 v/v). Powder of the desired compound (0.06 g, 0.10 mmol) was obtained in 9% yield.

The NMR and mass spectra are reported in the ESI (Fig. S1, S2 and S3†).

^{1}H-NMR (CDCl₃) δ ppm: 8.24 (2H, Ph-H, d, $J = 8.8$ Hz), 7.66 (2H, Ph-H, d, $J = 9.2$ Hz), 7.42 (2H, Ph-H, d, $J = 8.8$ Hz), 7.41 (1H, Th-H, s), 7.08 (1H, Th-H, s), 6.80 (2H, Ph-H, br d, $J = 7.8$ Hz), 3.00 (6H, –N(CH₃)₂, s), 2.05 (3H, Th-CH₃, s), 1.98 (3H, Th-CH₃, s).

^{13}C-NMR (101 MHz, CDCl₃) δ ppm: 146.90, 144.18, 143.19, 139.44, 139.26, 126.79, 126.65, 125.82, 125.43, 125.29, 124.50, 120.04, 112.96, 14.73, 14.48.
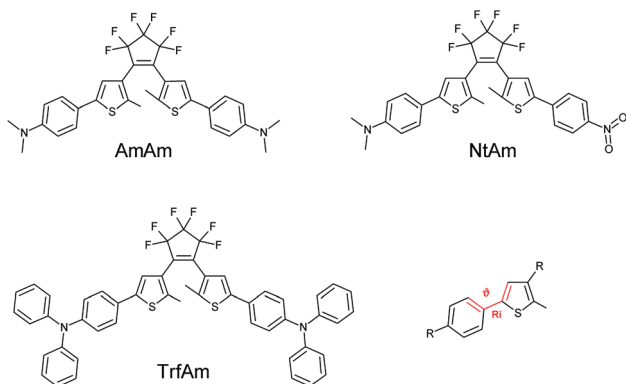
ESI-MS: m/z 609.1 [M + H⁺].

Fig. 1 Molecular structure of the studied molecules: **AmAm**: symmetric with amino groups, **NtAm**: asymmetric with nitro and amino groups, **TrfAm**: symmetric with diphenylamine groups. The bond length R_i and the dihedral angle θ are also reported.

TrfAm. 1,2-Bis-(5-chloro-2-methyl-3-thienyl)hexafluorocyclopentene (0.600 g, 1.37 mmol), 4-(diphenylamino)phenylboronic acid (1.07 g, 3.70 mmol), Pd(PPh$_3$)$_4$ (0.210 g, 0.182 mmol) in 9 mL of degassed toluene, and 6 mL of a degassed 2 M aqueous Na$_2$CO$_3$ solution were refluxed under argon for 40 hours. The mixture was extracted with dichloromethane : water. The combined organic layer was dried over Na$_2$SO$_4$, filtered and, after solvent removal, the raw product was purified by flash chromatography on silica gel (hexane : dichloromethane, 8 : 2 v/v) to give 550 mg of the desired product in 47% yield.

^{1}H-NMR (CDCl$_3$) δ ppm: 7.39 (4H, Ph-H, d, J = 8.6 Hz), 7.27 (8H, Ph-H, dd, J = 7.3 Hz, J = 8.4 Hz) 7.17 (2H, Th-H, s), 7.11 (8H, Ph-H, d, J = 7.6 Hz), 7.05 (two signals overlapping, 8H, Ph-H, d, J = 8.4 Hz), 1.96 (6H, –CH$_3$, s).

^{13}C-NMR (101 MHz, CDCl$_3$) δ ppm: 147.68, 147.39, 142.11, 140.41, 129.36, 127.27, 126.43, 125.87, 124.61, 123.53, 123.28, 121.44, 14.55.

ESI-MS: m/z 854.2 [M$^+$].

The molecules were converted to the closed form by means of UV illumination at 311 nm (Philips PL-S 9W/01). The back conversion was obtained using a halogen lamp filtered with a Schott OF570 longpass filter.

The three molecules have been chosen to produce thin films in cellulose acetate butyrate, CAB matrix (Eastman CAB-531-1) on silicon substrates for the study of the complex refraction index and on BK7 glass substrates to analyse the transparency modulation. The films have been obtained starting from a solution of butyl acetate (80% v/v) and chloroform (20% v/v) containing a concentration of CAB (3% wt/v for the modulation of refractive index and 9% for the modulation of transparency) and different concentrations of photochromic molecules. The films were obtained by spin coating (POLOS 200), using different revolution speed for the two substrates: 300–500 rpm in the case of silicon, obtaining thicknesses of 300/500 nm; 600–700 rpm in the case of BK7 obtaining a thickness of approximately 3 μm.

Quantum chemical calculations

Density functional theory (DFT) calculations were carried out on both open and closed forms for the evaluation of the equilibrium geometry, the normal modes of vibration, the IR spectrum and the electronic molecular polarisability at static electric field. We employed the B3LYP/6-31G(d,p) method and the quantum chemistry code Gaussian.[34]

Spectroscopic and ellipsometry characterisation

The measurements of the light absorption properties of the photochromic solutions and films were performed with a Jasco V570 UV-Vis-NIR spectrometer. The absorption spectra are reported here as molar extinction coefficient ε (M^{-1} cm^{-1}). The IR absorption spectra were collected with a Nicolet FT-IR spectrophotometer Magna IR 560 (64 scan, 2 cm^{-1} resolution), drop casting the molecules from solution on a ZnSe substrate. The spectra were then analysed with Omnic 7.1 software.

Spectroscopic ellipsometry measurements were performed with a rotating compensator instrument (M2000, J.A. Wollam

Co., Inc) and analysed using the VASE software. The measurements were carried out at incident angles of 60°, 65° and 70°.

The well-known, simple Cauchy model was found to fit data in the transparent region (null extinction), 1000–1700 nm. The real part of the refraction index and the extinction coefficient have been obtained by applying a multi-oscillator model to data in the 500–1700 nm range.[26]

Design and writing of computer generated holograms (CGH)

The CGHs adopted in this paper are Fresnel holograms calculated starting from black and white images as reported in the literature.[35]

The calculated binary pattern was then transferred by means of a direct-laser writing machine[36] equipped with visible lasers. The photochromic film is first completely converted to the coloured form by means of UV illumination, then the visible laser (638 nm, nominal power of 15 mW) is focused onto the film to convert it locally to the transparent form.

For the hologram reconstruction, a He–Ne laser (633 nm) was employed in case of amplitude reconstruction. The images were collected by a CCD camera (Thorlabs DCC1545M).

For the measurement of the diffraction efficiency of gratings, we used a tuneable Xenon light source (Newport TLS130B-300X). The wavelength was scanned from 500 to 1000 nm and sent through the grating at normal incidence. The diffracted light was measured by a silicon photodiode (Thorlabs S130VC) at the corresponding diffraction angle. The same measurement was performed without the grating to have the total intensity. The ratio of the two measurements was the efficiency.

Interferometry has been applied to measure the pattern distortion of the grating by means of a Zygo GPI interferometer.

Results and discussion

In this section, we report the results of our investigation. We start from the outcomes of the DFT calculations; then, we show the spectroscopic (UV-Vis/IR) characterisation of the solutions and films, and finally we report and discuss the results of the holographic writing.

Molecular structure

Table 1 reports the dihedral angle θ between the thiophene ring and the phenyl ring (see Fig. 1 for the definition).

Table 1 Dihedral angle θ between the thienyl ring and the phenyl ring of the three diarylethenes. In the case of **NtAm**, the contributions of the substitute nitro and amino are reported separately

	Dihedral angles θ (deg)					
	θ open		θ close		$\Delta\theta$	
AmAm	25.1°		9.5°		15.3°	
TrfAm	24.7°		12.3°		12.4°	
NtAm	Am	Nt	Am	Nt	Am	Nt
	25.2°	20.8°	5.0°	15.2°	20.2°	5.6°

Table 2 Bond length R_i between the two aromatic rings of the three diarylethenes investigated in this work. For the **NtAm** molecule the lengths of the R_i bonds located on the nitro and amino sides are reported individually

	Bond length R_i (Å)					
	R_i open		R_i close		ΔR_i	
AmAm	1.465		1.455		0.010	
TrfAm	1.465		1.457		0.008	
NtAm	Am	Nt	Am	Nt	Am	Nt
	1.464	1.464	1.452	1.462	0.012	0.002

θ is larger in the open form than in the closed form, in agreement with previous works.[37] Such increase of the planarity of the molecule in the closed form leads to more effective π conjugation that competes with the steric hindrance of the facing hydrogen atoms of phenyl and thienyl rings.[37] A further analysis reveals that the θ angle is larger in the open form when a donor group (Am) is present instead of an acceptor group (Nt). This is consistent with the increase of electron density on the phenyl ring caused by the donor, which increases the steric hindrance. Remarkably, switching to the closed form, the decrease of the θ angle (*i.e.*, the planarisation of the molecule) is more pronounced in the molecules with donor groups. Interestingly, the largest change occurs in the asymmetric molecule (**NtAm**) on the amino side (Am) – see Table 1. This is not surprising since, in the closed form, the presence of the push–pull structure enhances charge transfer and π-delocalization through the whole molecule. Therefore, in this peculiar case (**NtAm**), a reduction of 20° in the θ angle occurs, with a final value of about 5°, which corresponds to an almost planar structure.

The inter-ring bond length R_i (Table 2) follows a trend consistent with that of the angle θ: R_i shortens on passing from the open to the closed form. This means that the single bond partially acquires a double bond character in the closed form, in relation with the increased effectiveness of π-delocalization.

We are interested in the evaluation of the refractive index; therefore, we calculated the molecular polarisability tensor (α) since the macroscopic refractive index depends on it.[38] From the DFT calculations of α we obtained the average molecular polarisability, $P = (\alpha_{xx} + \alpha_{yy} + \alpha_{zz})/3$, and the average polarisability contribution per electron, PPE = P/Z (where Z is the

sum of the atomic numbers of the molecule). The values of P and PPE are reported in Table 3. In the closed form, polarisabilities are always larger than in the open form. As already pointed out, upon photoisomerisation, the delocalization path of π electrons increases. This leads to the increase of polarisability, in agreement with literature.[37,39] Accordingly, as shown in Table 3, we observe polarisability increments in the range 20–30%. The largest polarisability change occurs in **TrfAm**, thanks to the presence of the three phenyl rings on each side. The ΔPPE is even more interesting: this quantity reflects the specific increase of the electronic π-delocalization. We notice that the largest ΔPPE occurs in the push–pull structure (0.45 bohr³),
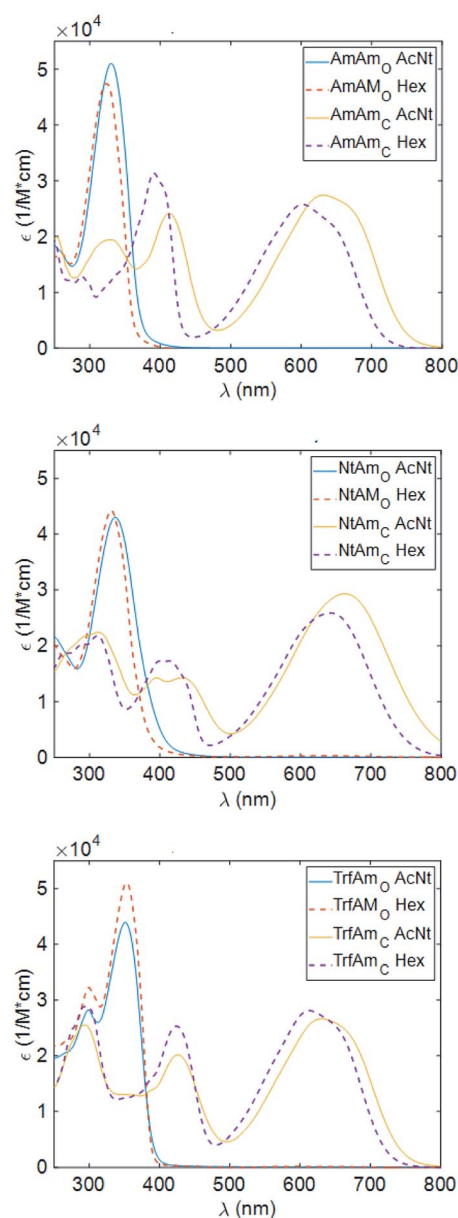
Fig. 2 Wavelength dependence of the molar extinction coefficients (ε) of the three molecules in their open (uncoloured, O) and closed (coloured, C) forms. We report data for solutions in acetonitrile (continuous lines) and hexane (dotted lines) calculated from ~10^{-5} M solutions.

Table 3 Molecular polarizabilities ($P = 1/3\mathrm{Tr}\alpha$) and the corresponding single electron contribution (PPE = P/Z) from DFT calculation for the three diarylethenes under study, in open and closed form

	Polarizability P (bohr³)			PPE (bohr³)		
	P_O	P_C	ΔP	PPE$_O$	PPE$_C$	ΔPPE
AmAm	446	579	133	1.42	1.84	0.42
NtAm	429	569	140	1.37	1.82	0.45
TrfAm	694	876	182	1.57	1.98	0.41

whereas the two symmetric amine-based molecules show a smaller value ($\sim$0.4 bohr^3).

Characterisation in solution and thin film

We show in Fig. 2 the UV/Vis absorption of the open and closed forms of the three diarylethenes in solution state (acetonitrile and hexane solvents). Table 4 reports the wavelength position of the absorption peaks with the corresponding molar extinction coefficients.

Considering the spectra of the open forms, we do not identify large differences between hexane and acetonitrile. We observe a small bathochromic effect increasing the polarity of the solvent,[40,41] with **NtAm** showing a more pronounced effect.

The situation dramatically changes in the coloured form, the bathochromic effect is large, especially for **AmAm** and **NtAm**. As for the molar extinction coefficient ε, the three derivatives show values of the order of 30 000 M^{-1} cm^{-1}. They are very large if compared with those of systems based on the same phenyl-thienyl perfluorocyclopentene structure, that are in the 10 000–20 000 M^{-1} cm^{-1} range, depending on the enhancement of the π extension.[35,42] We also notice the large intensity of the secondary peak in the region 400–450 nm for the coloured form of **AmAm** and **TrfAm** and its shape is different in the two solvents. Such large values will turn into high contrast values in transparency for polymeric films doped with such molecules.

The three derivatives were added to the CAB for the production of thin films on silicon and quartz substrates. In Fig. 3, we report the wavelength dependence of the extinction coefficients of such films cast on quartz substrates.

The peak position (λ_o) and the corresponding molar extinction (ε_o) of the CAB films doped with the three diarylethene derivatives are reported in Table 5.

It is worth noting that the molar extinction coefficients are very similar in acetonitrile and in CAB films (see Tables 4 and 5 for comparison).

Infrared spectra

Infrared spectroscopy has been used in the past to study the chemical structure of diarylethenes and the effect of the substituents.[37,43] For this purpose, the IR spectra of the three diarylethenes in open and closed form were recorded and compared to the spectra simulated from DFT calculations. We focused on the 1700–700 cm^{-1} spectral range, where we observe the largest differences between the open and closed form. We
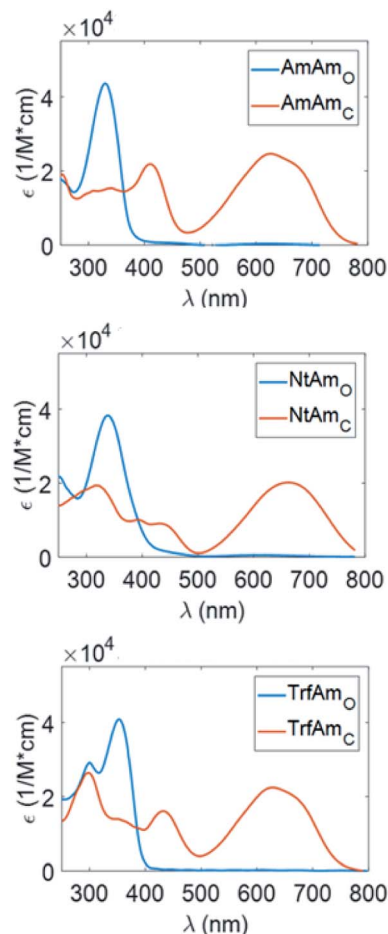

Fig. 3 Molar extinction coefficients, ε, for the three films in open, uncoloured, and closed, coloured, forms, containing CAB and molecules under study (from left to right: **AmAm** 1710^{-4} mol cm^{-3}, **NtAm** 1610^{-4} mol cm^{-3} and **TrfAm** 1210^{-4} mol cm^{-3}).

report in Fig. 4 the simulated and experimental IR spectra of **AmAm** (the spectra of the other two derivatives are in the ESI, Fig. S4†). We notice the good agreement of the theoretical spectra with their experimental counterparts.

While going from the open to the closed form we observe a redshift of the collective CC stretching mode of the backbone, which is assigned to the intense band at $\sim$1600 cm^{-1}. Another band with similar behaviour is observed at about 1500 cm^{-1}, which is consistent with the results reported in the literature for analogous systems.[44,45]

Table 4 Absorption maxima (nm), molar extinction coefficients (10^4 M^{-1} cm^{-1}) and quantum yield for investigated diarylethenes in acetonitrile and hexane solution

	Acetonitrile					Hexane				
	λ_o	ε_o	λ_c	ε_c	$\Phi_{O\to C}$	λ_o	ε_o	λ_c	ε_c	$\Phi_{O\to C}$
AmAm	330	4.94	635	2.94	0.02	324	4.58	607	2.22	0.79
NtAm	336	4.30	663	2.93	0.09	330	4.42	640	2.58	0.57
TrfAm	351	4.40	630	2.78	0.37	353	5.10	613	2.81	0.62

Table 5 Absorption maxima (nm) and molar extinction coefficients (10^4 M^{-1} cm^{-1}) for film with CAB and the different diarylethenes

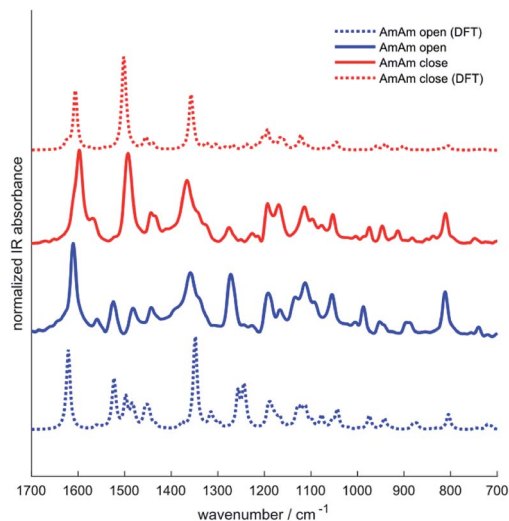|	Film CAB + molecule			
	λ_o	ε_o	λ_c	ε_c
AmAm	330	4.35	627	2.46
NtAm	339	3.83	660	2.01
TrfAm	353	4.08	629	2.24

Fig. 4 IR spectra for **AmAm** in the range 1700 to 700 cm^{-1}: from top to bottom, calculated closed form, experimental closed form, experimental open form and calculated open form. To ease the comparison of the simulated spectra with their experimental counterparts we adopted an empirical scale factor of 0.97.

The inspection of the total IR intensities computed by DFT for the three derivatives in the two forms reveals an interesting effect (Table 6). A strong increase in the IR intensity occurs from the open to the closed form. The effect is remarkable for the **NtAm** derivative that has a strong push–pull character in the closed form, which drives a large increase of the IR intensity of the normal modes involving the CC stretching of the molecular backbone. Indeed, such modes are coupled with sizeable π electron density variations.

Another important information that can be achieved from the IR spectra is the degree of conversion of the diarylethenes from the uncoloured to the coloured forms. We identified a band around 910 cm^{-1}, which is assigned by DFT to the bending of the two –CH$_3$ groups linked to the thiophene rings. The inspection of this band allows monitoring the photochromic conversion because this band shifts to higher

Table 6 Determination of the conversion degree from open to closed form from the experimental IR spectra of the three investigated diarylethenes (Fig. 4 and S1). The IR intensity ratio (I_C/I_O) and the IR intensity difference ($\Delta I = I_C - I_O$) between the closed and open forms of the three diarylethenes are taken from DFT calculations as the sum of the intensities of all the normal modes. The conversion degree has been calculated as the ratio of the area of the band at 910 cm^{-1} in the close and open form: A_C/A_O

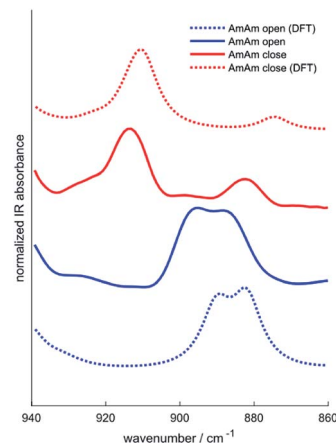| | Conversion degree and intensity IR, I [km mol^{-1}] | | | |
	Conversion degree	I_{tot} open	I_{tot} closed	I_c/I_o	ΔI
AmAm	98.7%	5652.8	10 660.5	1.88	5007.6
NtAm	98.8%	5457.1	11 386.4	2.09	5929.3
TrfAm	87.7%	6407.3	11 863.8	1.85	5456.4

Fig. 5 IR spectra for **AmAm** in between 940 to 860 cm^{-1}: from top to bottom, calculated closed form, experimental closed form, experimental open form and calculated open form. To ease the comparison of the simulated spectra with their experimental counterparts we adopted an empirical scale factor of 0.98.

wavenumbers when going from the open to the closed form – see for instance the spectra of **AmAm** shown in Fig. 5.

When there is a complete conversion of the photochromic system the doublet of the open form disappears. This behaviour is common to all the molecules. The degree of conversion determined by IR spectroscopy of the 910 cm^{-1} band is reported in Table 6 with its definition. Such values are consistent with many diarylethene derivatives[40,46–48] and with those bearing the same perfluorodithienylcyclopentene core,[42] that show a degree of conversion of about 100% at the photostationary state in different solvents.

Modulation of transparency

Photochromic materials, in particular diarylethenes, have an important modulation of transparency:[18,24,27] the systems described in this paper have the same feature according to the results obtained in solution. In order to quantify the modulation of transparency, we define the contrast as the ratio of transmittance between the uncoloured (open) and coloured (closed) forms:

$$C = \frac{T_o(\lambda)}{T_c(\lambda)} = \frac{1}{10^{-A_c(\lambda)}} \qquad (1)$$

The visible band is the most important spectral region for applications, for instance, in holography.[35] In this region, only the closed form has an absorption, therefore the visible contrast depends on the absorbance of the closed form, $A_c(\lambda)$, as shown in eqn (1). It is therefore necessary to have films with a very high absorption in the visible. In the case of amplitude CGH, the efficiency is directly dependent on the contrast and values larger than 10^2 are required at the wavelength selected for the hologram reconstruction,[28] for other applications that exploit a wider spectral range, such requirement must be extended to the target region.

Table 7 Parameters of the four films under consideration: concentration of diarylethene on CAB's array, thickness, absorbance of films on closed form and contrast at 633 nm, reading wavelength of holograms

Film	Molecule	Concentration	d (μm)	Abs closed form [633 nm]	Contrast, C [633 nm]
1	**TrfAm**	16.2%	3.7	2.5	326.5
2	**AmAm**	16.6%	3.7	2.8	584.6
3	**AmAm**	16.6%	4.4	3.6	3919
4	**AmAm**	18.7%	2.8	2.8	828.5

In accordance with this requirement, CAB films doped with **AmAm** and **TrfAm** derivatives were obtained on BK7 glass substrates. The details of the films are reported in Table 7.

One can see that the solubility of the photochromic molecules in CAB matrix is large. Such feature together with the large absorption coefficient of the closed form in the visible makes it possible to obtain large absorption and contrast in films with a thickness of a few μm. This is important, since it is easier to preserve a good optical quality in thin films.

In Fig. 6, the spectra of Film 1 containing 16.2% of **TrfAm** are reported together with the contrast function for the same film.

We notice that the contrast threshold of 100 is exceeded in a spectral region of about 100 nm centred at 600 nm. Bearing in mind that this is the film with the lowest value of contrast, this means that is not difficult to have films matching the requirements of having efficient amplitude holograms and optical devices based on contrast in the visible.

Modulation of the refractive index

The modulation in transparency is suitable for amplitude holograms, whereas the modulation of the real part of the refractive index is crucial in order to have volume phase holograms.[49]

The two key parameters that guide the refractive index and its change upon photoisomerisation are the molecular polarisability and the concentration of the photochromic moiety.[35]
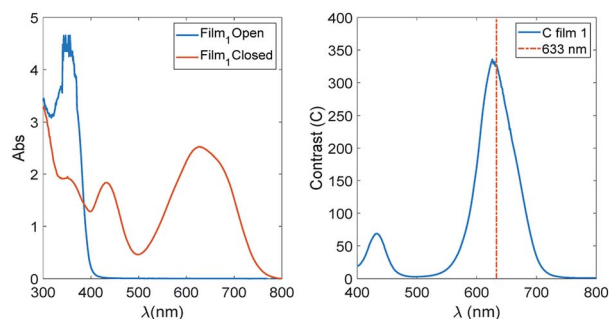

Fig. 6 Left: Absorption spectra for Film 1 with 16.2% of **TrfAm** in both open and closed forms. Right: Contrast function of Film 1. The dotted line at 633 nm identifies the wavelength used to reconstruct the holograms.

Here, we exploited spectroscopic ellipsometry[50] to determine the optical properties and in particular the refractive index of films contained CAB's matrix and different concentration of **AmAm**, **NtAm** and **TrfAm** deposited on silicon substrates in open and closed form.

We expect that the photochromic film can be described by multi-oscillator models with a trend of the refractive index reported in the literature:[18] the open form does not absorb in the visible and in the NIR range, but only in the UV (see discussion of Fig. 3 for the films on quartz). In this situation, the extinction is null ($\kappa = 0$) and the real part of refractive index has a normal dispersion (see Fig. 7, top left). Instead, in the closed form (Fig. 7, top right), the normal dispersion is only present in the NIR range, because the structure is coloured and absorbs in the visible ($\kappa > 0$).

To evaluate the dispersion curve of the real part of the refractive index, we selected a 2-terms Cauchy model to fit the data over the 1000–1700 nm range. Pure CAB films were used to determine the refractive index of the matrix and such value was used as a reference. In the bottom of Fig. 7, we show the refractive index at 1000 nm of CAB films doped with different amounts of the **AmAm** dye, together with the dispersion curve of Δn calculated as the refractive index difference between the closed and the open forms.

We report in Table 8 the values of the A and B parameters of the Cauchy model, the corresponding refractive index (n), and the refractive index difference $\Delta n = n_C - n_O$ at 1000 nm for all concentrations. We observe a huge increase of the B parameter going from the open to the closed form. The B parameter is related to the dispersion and it is mainly dependent on the presence and position of the absorption band in the visible. Furthermore, we also observe a linear relationship of the refractive index with the concentration of the dye. The slope is
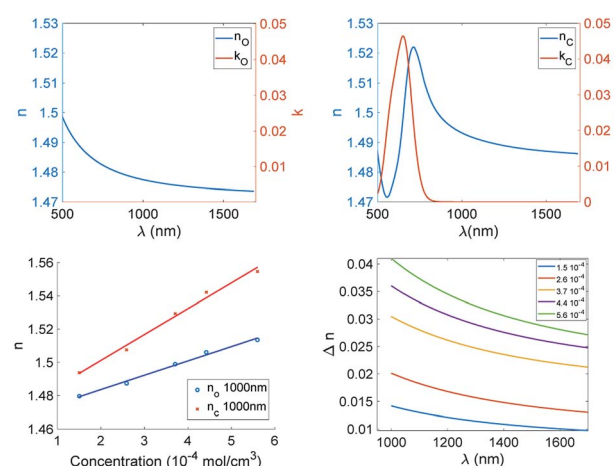

Fig. 7 Top: Complex refractive index for the open (left panel) and closed (right panel) forms of the **AmAm** doped CAB film (the plots of the other two derivatives are reported in Fig. S5†). Bottom: (left panel) The real part of the refractive index at 1000 nm in the open and closed forms as a function of the molar concentration of **AmAm** in CAB; (right panel) refractive index difference ($\Delta n = n_C - n_O$) as function of the wavelength.

Table 8 Summary of Cauchy model fitting of ellipsometry data in the NIR range for CAB films of the three derivatives investigated. A and B are the Cauchy model coefficients and n the corresponding refractive index at 1000 nm. Δn is the refractive index difference between closed and open forms

C molar [10^{-4} mol cm^{-3}]	Form	A	B [10^4 nm^2]	n, 1000 nm	Δn, 1000 nm
AmAm					
1.5	Open	1.473	0.667	1.480	0.014
	Closed	1.480	1.346	1.494	
2.6	Open	1.479	0.886	1.487	0.020
	Closed	1.488	1.975	1.508	
3.7	Open	1.489	0.966	1.499	0.030
	Closed	1.506	2.377	1.529	
4.4	Open	1.494	1.162	1.506	0.036
	Closed	1.513	2.883	1.542	
5.6	Open	1.503	1.088	1.514	0.041
	Closed	1.522	3.207	1.555	
NtAm					
1.6	Open	1.474	0.887	1.483	0.013
	Closed	1.480	1.558	1.496	
2.5	Open	1.483	0.727	1.491	0.024
	Closed	1.495	1.968	1.514	
4.3	Open	1.492	0.874	1.501	0.030
	Closed	1.506	2.571	1.531	
TrfAm					
1.2	Open	1.474	1.149	1.485	0.008
	Closed	1.478	1.537	1.493	
2.3	Open	1.490	0.783	1.498	0.016
	Closed	1.499	1.538	1.514	
3.2	Open	1.500	1.154	1.511	0.023
	Closed	1.511	2.329	1.534	

Fig. 8 Trends of Δn at 1000 nm of CAB films as function of molar concentration of the three photochromic derivatives.

much larger for the coloured form. This is expected since both the A and B values of the Cauchy formula increase with the concentration. This is due to the combination of the increase of polarisability going from the open to the closed form and to the pre-resonance effect which is more pronounced in the coloured form.

This trend is common to the three derivatives. To better understand the difference among such diarylethenes, we plot the modulation of the refractive index at 1000 nm as a function of dye concentration (Fig. 8).

It is clear that the dye concentration is the driving parameter inducing the modulation of the refractive index, and just small differences show up among the three diarylethenes investigated here.

The modulation of the refractive index in the NIR is very large and such values were achieved in the past only in backbone photochromic polymers[18,24,26] indicating that a suitable combination of soluble derivative in a polymer matrix and a large modulation of polarisability induced by electroactive substituents is a winning strategy. We can conclude that efficient phase holograms can be obtained with such systems.
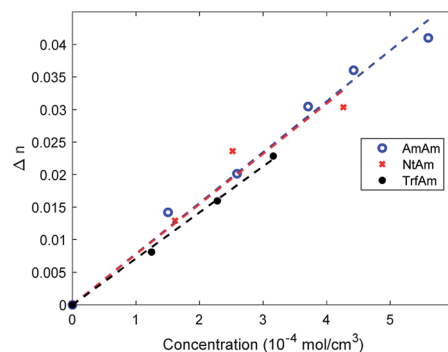
Holographic writing and reconstruction

To test the capability of writing photochromic holograms, we started with a diffraction grating, which can be considered as the simplest hologram. We wrote on Film 2 (see Table 7) a 10 mm × 10 mm grating with a line density of 125 L mm^{-1} and a duty cycle of 50%. The procedure for the device manufacturing is reported in Materials and methods. In Fig. 9, the microscope image of the pattern is reported.

We notice the good quality of the pattern; moreover, the measured value of the duty cycle (DC) was 45%, very close to the design value of 50%.

The pattern distortion has been evaluated by using a null interferometer with a plane reference. Indeed, by measuring the 0, −1 and +1 orders, it is possible to separate the component of the wave front due to the pattern defects and to the surface distortion.[51] The RMS error in the pattern writing is 0.1 μm, which is low and confirms the high precision of the direct writing machine.

The diffraction efficiency of the +1 order was measured as function of the wavelength and light polarization. The plot is reported in Fig. 10.

Considering the absorption properties of the film, we can say that the grating is a pure phase grating at long wavelengths and it becomes a mix of amplitude and phase grating below 800 nm. We see how the efficiency increases from 1000 nm to shorter wavelengths[52] and this is consistent with the increase of the
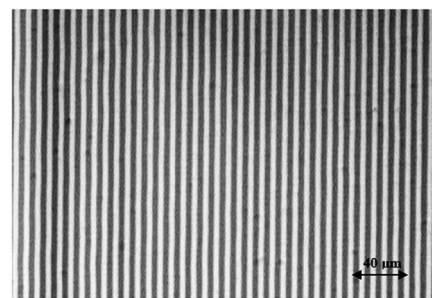

Fig. 9 Microscope image of the binary grating written on Film 2 with photochromic **AmAm** collected by means of a standard optical microscope.
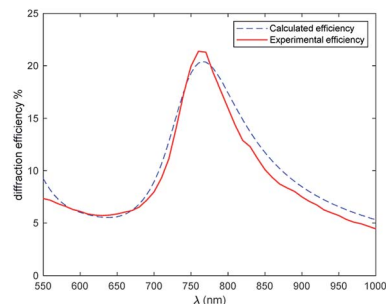
Fig. 10 Diffraction efficiency of the 1st order from 550 to 1000 nm experimental and calculated.

Fig. 12 Top: Frames to achieve origin of first order focus of Fresnel lens. Bottom: Images of the focus spot for the three diffraction orders.

modulation of the refractive index. Remarkable values of about 22% are measured at about 770 nm, then the efficiency drops quickly because of the increase in the absorption component and a corresponding decrease of Δn, due to the anomalous dispersion of the coloured form. Values of the order of 6% are measured around 630 nm, then, at shorter wavelength, the efficiency slightly increases since the absorption decreases and Δn is not negligible (the closed form shows a low index). The curve can be modelled by means of an RCWA approach, as shown in Fig. 10. We notice the good agreement with the experimental results.

The step forward has been the writing of a Fresnel lens on Film 1, which is doped with **TrfAm** molecule. The lens was designed to have a diameter of 7 mm and a focal length of 20 cm. In Fig. 11, two images of the CGH Fresnel lens are reported.

The pattern was illuminated with a collimated red laser at 633 nm and the intensity of the focused spot was measured with a photo-diode, providing a diffraction efficiency of 6.7% in the first order.

A CCD camera has been also used to determine the focal position as reported in the top panels of Fig. 12, and the value of 20 cm was confirmed. In addition, we also recorded frames of first, second and third orders at the focal lengths L, $L/2$ and $L/3$, respectively (bottom panels of Fig. 12).

The size of the focal spot decreases going from the first to the third order. This is consistent with the fact that the focal ratio $F\# = L/D$ decreases (L and D are the focal length and the diameter of Fresnel lens, respectively).

To prove the quality of the writing setup and of the substrate, we realized two Fresnel CGHs of two images using Film 2 and Film 3. In Fig. 13, the starting images, the corresponding

Fig. 13 Top: Starting images, left (Owl) and right (Deer). In the middle: the two calculated CGH corresponding to image. Bottom: The two reconstruction CGHs at focal length 50 cm and collimated beam at 633 nm; the images are recorded with a CCD camera.
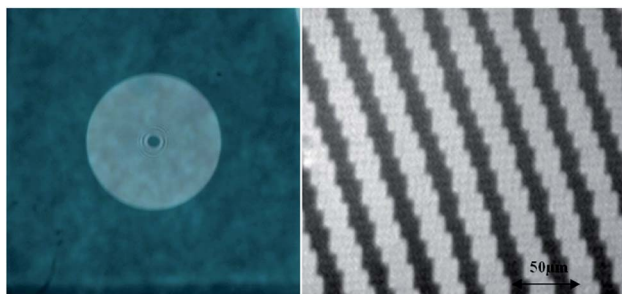

Fig. 11 Left: Photo of the Fresnel lens written on the photochromic film; Right: Detail of Fresnel pattern recorded with a standard optic microscope.
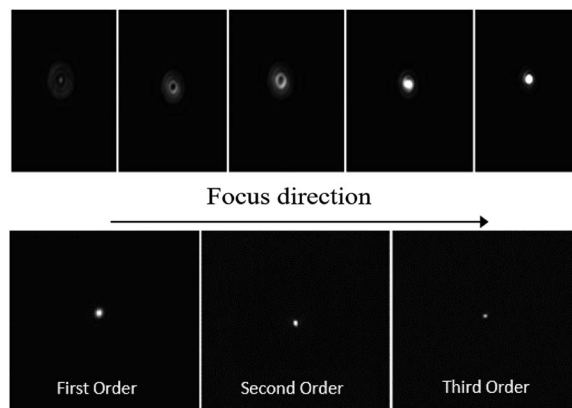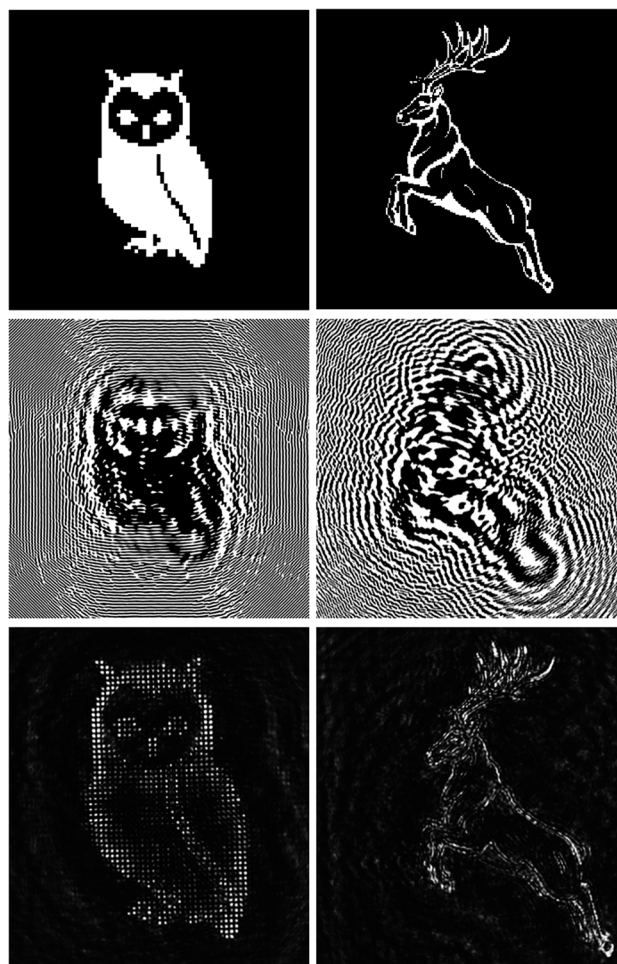
calculated CGHs and the reconstructed images (at 633 nm) of an owl (Film 1) and a deer (Film 2) are reported.

The overall size of the holograms is 8 mm × 8 mm, the pixel size is 4 μm and in both cases the reconstructed image is 4 mm × 4 mm at a focal distance of 500 mm. However, the pixel sizes of the reconstructed images are different: 40 μm and 13 μm for the owl and the deer respectively. We notice that the reconstruction quality is in general high, with better details in the case of the owl. This is due to the fact that the deer has many tiny details that could be reconstructed only if the CGH had a larger resolution.

Conclusions

In this paper we studied three dithienylethene derivatives bearing both donor and acceptor groups with a unique combination of high solubility in CAB matrix and a large change in molecular properties. The UV-vis characterisation in solution showed the large absorption coefficients of the derivatives with at least one donor group. Looking at the equilibrium geometries, it is apparent how the increase in π conjugation going from the open to the closed form is enhanced when a D–A structure is present, which occurs for the nitro–dimethylamino compound (**NtAm**). This behaviour is due to the push–pull character of **NtAm**. Considering IR spectroscopy, we have shown that the increase of absorption intensity can reach a factor of two when going from the open to the closed form of **NtAm**. Based on IR spectroscopy in solution state we have also proved an almost total photoconversion between the two forms. CAB-based films doped with the photochromic derivatives were obtained and a very good solubility of the derivatives in the polymer matrix was found. This is crucial since it allowed increasing the doping level thus achieving, even for thin films, a large modulation of the transparency in the visible and a large change of the refractive index in the NIR (Δn). Such high response films were used as substrates for CGHs, starting from grating to images. It has been proved that the holograms can work both in amplitude (in the visible) and in phase (in the NIR) providing efficiencies larger than 20%. We can therefore consider such polymer films as rewritable films with very appealing potential in high performance hologram manufacturing.

Conflicts of interest

There are no conflicts to declare.

Acknowledgements

Notes and references

1 A. Bianco, S. Perissinotto, M. Garbugli, G. Lanzani and C. Bertarelli, *Laser Photonics Rev.*, 2011, **5**, 711–736.

2 S. Ishida, D. Kitagawa, S. Kobatake, S. Kim, S. Kurihara and T. Fukaminato, *Chem. Commun.*, 2019, **55**, 5681–5684.

3 T. Fukaminato, S. Ishida and R. Métivier, *NPG Asia Mater.*, 2018, **10**, 859–881.

4 A. Fernandez-Acebes and J. M. Lehn, *Chem.–Eur. J.*, 1999, **5**, 3285–3292.

5 D. Kim, K. Jeong, J. E. Kwon, H. Park, S. Lee, S. Kim and S. Y. Park, *Nat. Commun.*, 2019, **10**, 3089.

6 Y. Arai, S. Ito, H. Fujita, Y. Yoneda, T. Kaji, S. Takei, R. Kashihara, M. Morimoto, M. Irie and H. Miyasaka, *Chem. Commun.*, 2017, **53**, 4066–4069.

7 R. Kajiya, S. Sakakibara, H. Ikawa, K. Higashiguchi, K. Matsuda, H. Wada, K. Kuroda and A. Shimojima, *Chem. Mater.*, 2019, **31**, 9372–9378.

8 F. Tong, D. Kitagawa, X. Dong, S. Kobatake and C. J. Bardeen, *Nanoscale*, 2018, **10**, 3393–3398.

9 *Mechanically Responsive Materials for Soft Robotics*, ed. H. Koshima, John Wiley & Sons, 2020.

10 W. A. Velema, W. Szymanski and B. L. Feringa, *J. Am. Chem. Soc.*, 2014, **136**, 2178–2191.

11 P. D. Bregestovski and G. V. Maleeva, *Neurosci. Behav. Physiol.*, 2019, **49**, 184–191.

12 H. F. O. Müller, *Renewable Energy*, 1994, **5**, 935–941.

13 J.-A. Piao, M.-L. Piao, E.-S. Kim and N. Kim, *Proc. SPIE*, 2013, **8644**, 864419.

14 F.-K. Bruder, F. Deuber, T. Faecke, R. Hagen, D. Hoenel, D. Jurbergs, M. Kogure, T. Roelle and M.-S. Weiser, *J. Photopolym. Sci. Technol.*, 2009, **22**, 257–260.

15 D. H. Close, *Opt. Eng.*, 1975, **14**, 145402.

16 B. R. Brown and A. W. Lohmann, *IBM J. Res. Dev.*, 1969, **13**, 160–168.

17 H. Kogelnik, *Bell Syst. Tech. J.*, 1969, **48**, 2909–2947.

18 C. Bertarelli, A. Bianco, R. Castagna and G. Pariani, *J. Photochem. Photobiol., C*, 2011, **12**, 106–125.

19 M. Hanazawa, R. Sumiya, Y. Horikawa and M. Irie, *J. Chem. Soc., Chem. Commun.*, 1992, 206–207.

20 S. Nakamura and M. Irie, *J. Org. Chem.*, 1988, **53**, 6136–6138.

21 M. Irie, T. Fukaminato, K. Matsuda and S. Kobatake, *Chem. Rev.*, 2014, **114**, 12174–12277.

22 Q. Luo, H. Cheng and H. Tian, *Polym. Chem.*, 2011, **2**, 2435–2443.

23 T. J. Wigglesworth, A. J. Myles and N. R. Branda, *Eur. J. Org. Chem.*, 2005, 1233–1238.

24 L. Oggioni, C. Toccafondi, G. Pariani, L. Colella, M. Canepa, C. Bertarelli and A. Bianco, *Polymers*, 2017, **9**, 462.

25 G. Pariani, R. Castagna, G. Dassa, S. Hermes, C. Vailati, A. Bianco and C. Bertarelli, *J. Mater. Chem.*, 2011, **21**, 13223–13231.

26 C. Toccafondi, L. Occhi, O. Cavalleri, A. Penco, R. Castagna, A. Bianco, C. Bertarelli, D. Comoretto and M. Canepa, *J. Mater. Chem. C*, 2014, **2**, 4692–4698.

27 A. Bianco, C. Bertarelli, R. Castagna, G. Pariani and A. Zanutta, *Proc. SPIE*, 2012, **8281**, 828104.

28 G. Pariani, C. Bertarelli, G. Dassa, A. Bianco and G. Zerbi, *Opt. Express*, 2011, **19**, 4536–4541.

29 S. Lee, Y. You, K. Ohkubo, S. Fukuzumi and W. Nam, *Chem. Sci.*, 2014, **5**, 1463–1474.

30 H. Wan, H. Xue, Y. Ling, Y. Qiao, Y. Chen and G. Zhou, *Phys. Chem. Chem. Phys.*, 2018, **20**, 14348–14356.

31 K. J. Chen, A. D. Laurent and D. Jacquemin, *J. Phys. Chem. C*, 2014, **118**, 4334–4345.

32 S. Hermes, G. Dassa, G. Toso, A. Bianco, C. Bertarelli and G. Zerbi, *Tetrahedron Lett.*, 2009, **50**, 1614–1617.

33 J. Yang, S. Liu, J.-F. Zheng and J. Steve Zhou, *Eur. J. Org. Chem.*, 2012, **2012**, 6248–6259.

34 M. J. Frisch, G. W. Trucks, H. B. Schlegel, G. E. Scuseria, M. A. Robb, J. R. Cheeseman, G. Scalmani, V. Barone, B. Mennucci, G. A. Petersson, H. Nakatsuji, M. Caricato, X. Li, H. P. Hratchian, A. F. Izmaylov, J. Bloino and G. Zhe, *Gaussian 09, Revision E.01*, 2009.

35 L. Oggioni, G. Pariani, C. Bertarelli and A. Bianco, *Materials*, 2019, **12**, 2810.

36 A. Bianco, M. Mantero, L. Oggioni, G. Pariani, C. Bertarelli and F. Zamkotsian, *Proc. SPIE*, 2019, **11030**, 110300B.

37 G. Callierotti, A. Bianco, C. Castiglioni, C. Bertarelli and G. Zerbi, *J. Phys. Chem. A*, 2008, **112**, 7473–7480.

38 C. J. F. Bottcher, *Theory of electric polarisation*, Elsevier, Amsterdam, 1952.

39 N. Adami, D. Fazzi, A. Bianco, C. Bertarelli and C. Castiglioni, *J. Photochem. Photobiol., A*, 2010, **214**, 61–68.

40 S. Kobatake, Y. Terakawa and H. Imagawa, *Tetrahedron*, 2009, **65**, 6104–6108.

41 H. H. Liu and Y. Chen, *J. Mater. Chem.*, 2011, **21**, 1246–1249.

42 J. J. D. de Jong, L. N. Lucas, R. Hania, A. Pugzlys, R. M. Kellogg, B. L. Feringa, K. Duppen and J. H. van Esch, *Eur. J. Org. Chem.*, 2003, **2003**, 1887–1893.

43 A. Takata, S. Yokojima, H. Nakagawa, Y. Matsuzawa, A. Murakami, S. Nakamura, M. Irie and K. Uchida, *J. Phys. Org. Chem.*, 2007, **20**, 998–1006.

44 A. Bianco, C. Bertarelli, J. F. Rabolt and G. Zerbi, *Chem. Mater.*, 2005, **17**, 869–874.

45 J. J. D. de Jong, W. R. Browne, M. Walko, L. N. Lucas, L. J. Barrett, J. J. McGarvey, J. H. van Esch and B. L. Feringa, *Org. Biomol. Chem.*, 2006, **4**, 2387–2392.

46 M. Irie, *Chem. Rev.*, 2000, **100**, 1685–1716.

47 M. Herder, B. M. Schmidt, L. Grubert, M. Pätzel, J. Schwarz and S. Hecht, *J. Am. Chem. Soc.*, 2015, **137**, 2738–2747.

48 S. Fredrich, R. Göstl, M. Herder, L. Grubert and S. Hecht, *Angew. Chem., Int. Ed.*, 2016, **55**, 1208–1212.

49 F. K. Bruder, R. Hagen, T. Rölle, M. S. Weiser and T. Fäcke, *Angew. Chem., Int. Ed.*, 2011, **50**, 4552–4573.

50 M. Canepa, in *Surface Science Technique*, ed. G. Bracco and B. Holst, Springer-Verlag, Heidelberg, 2013, pp. 99–135.

51 S. Reichelt, C. Pruss and H. J. Tiziani, *Proc. SPIE*, 2002, **4778**, 206–217.

52 A. Bianco, G. Pariani, C. Bertarelli and F. M. Zerbi, *Proc. SPIE*, 2010, **7739**, 77394P.